https://doi.org/10.5194/egusphere-2025-6421
Preprint. Discussion started: 27 January 2026

Linking ridge shapes to the ice thickness distribution via discrete element simulations

Marek Muchow[1], Einar Ólason[2], and Arttu Polojärvi[1]

[1]Aalto University, School of Engineering, Department of Mechanical Engineering, P.O. Box 14100, FI-00076 Aalto, Finland
[2]Nansen Environmental and Remote Sensing Center, Jahnebakken 3, Bergen, N-5007, Norway

Correspondence: Marek Muchow (marek.muchow@aalto.fi)

Abstract. Ridges significantly increase the sea-ice thickness compared to the level ice surrounding them. In continuum sea-ice models, this increase is either represented by an increase in mean ice thickness or by changes in the ice thickness distribution (ITD). The implementation of ITDs requires a sub-grid parametrization of ridging by using a redistribution scheme. In contrast, the discrete element method (DEM) enables explicit simulations of ridge formation process, including ice fragmentation into rubble and its subsequent redistribution to ridges. Here, we use a DEM model to simulate ridging across a sea ice domain of size $6\,\mathrm{km} \times 6\,\mathrm{km}$. The DEM simulations yield deformed ice cover with ridges of varying shapes, namely triangular and trapezoidal ridges; the trapezoidal ridges notably affect the ITD of the deformed ice cover by creating a bump in the ITD towards thicker ice. We find that the ITD of the deformed ice field from DEM simulations differs from those from the continuum model, that uses only mean thickness, and from two commonly used ridging functions within redistribution schemes used as sub-grid parametrizations. Further, we show how to formulate an analytical redistribution function that captures the effect of various ridge shapes and discuss when it could replace existing ridging schemes. Our results demonstrate that an improved representation of ridging is needed within continuum models to resolve ridges both with their depth and shape within the ITD, especially in high spatial resolutions. Additionally, we formulate open questions in need of answers to allow implementation of our new distribution of ridged ice into continuum models, which connect to the ridging process itself.

1 Introduction

Ridges present localized discontinuities in the sea-ice cover by significantly increasing the ice thickness locally. They are formed due to convergent sea-ice motion creating deformation and failure of the ice. Consequently, ice blocks pile on top of the ice and under the water, respectively forming the ridge sail and keel, and thus, thickening the ice. Overall, ridging has a higher influence on the ice volume via the thickness compared to the ice area (Mårtensson et al., 2012). For example, up to 36 % of the ice volume was covered by thick ridges during MOSAiC from fall 2019 to late summer 2020 (von Albedyll et al., 2022). In turn, ridges also influence the sea-ice motion and deformation: The sail and keel influence the atmosphere and

https://doi.org/10.5194/egusphere-2025-6421
Preprint. Discussion started: 27 January 2026

ocean drag, respectively, and the presence of ridges influences the large-scale ice-strength (Tuhkuri and Lensu, 2002; Martin et al., 2016; Tsamados et al., 2014; Brenner et al., 2021). Further, Krumpen et al. (2025) observed a rise in the annual number of ridging events due to an increase in first-year-ice fraction, indicating that ridging may become increasingly frequent and important in the future.

Despite their importance, the amount of thick and ridged ice is generally underestimated by conventional continuum sea-ice models (Johnson et al., 2012). Additionally, Bouchat et al. (2022) highlights that when comparing convergence from several models to satellite observations, only models running at a much higher resolution than the observed fields (10 km) were able to reproduce the observed convergence. As ridging requires convergent ice motion, the models may produce less ridges than expected. Further, Lipscomb et al. (2007) raised several questions regarding the assumptions of currently used ridging parametrizations, for example the shape of participation and redistribution function, which still remain open.

The representation of ridges in continuum models becomes even more important when they are adapted for high spatial and temporal resolutions, for example, for regional case studies, route planning, and operational forecast simulations (Blockley et al., 2020; Bouchat et al., 2022; Hutter et al., 2022; Williams et al., 2021). Especially for operational forecast simulations, the need for an accurate representation of ridges is emphasized, since ridged ice is one of the most common ice conditions where ships require ice-breaker assistance and where winter navigation accidents occur (Valdez Banda et al., 2015; Liu et al., 2024).

Continuum sea-ice models describe ridging as a sub-grid process. They describe the ice thickness either by using a two-level approach (Hibler, 1979) that only includes an open-water fraction and a mean ice thickness (e.g., neXtSIM (Ólason et al., 2022)) or with a multi-category thickness (e.g., CICE (Lipscomb et al., 2007; Hunke et al., 2010)). In the first case, ridging increases the mean ice thickness, whereas in the latter one, ridging is described by sea-ice redistribution functions and the ice thickness distribution (ITD). The redistribution functions include a participation function that governs which part of the ice deforms and a ridging function that determines to which thickness category the deformed ice belongs. The two common ridging functions are either based on Hibler (1980), assuming triangular ridges and linear redistribution of ice, or Lipscomb et al. (2007), assuming an exponential distribution of smaller ridges compared to deeper ridges.

In order to represent ridging more detailed than is possible in continuum models, we simulate ridging by using a discrete element method (DEM) model in this study, since it allows for detailed simulations of ridge formation processes (Hopkins, 1994, 1998; Muchow and Polojärvi, 2024). In DEM simulations of ridge formation processes, the intact sea ice is modeled by using particles connected by beams, which may fail and form ice blocks. Then, the ridging is simulated explicitly, including ice rubble formation and ice rubble accumulation. The code we use is the Helsinki Discrete Element Model (HiDEM) (Åström, 2006), which has demonstrated its capability to simulate sea-ice dynamics and fragmentation in three dimensions over kilometer-scale domains at meter-scale resolution (Åström and Polojärvi, 2024; Åström et al., 2024). Three dimensional modeling is required for realistic simulations including ridging (Muchow and Polojärvi, 2024).

The results presented here give insight into the ridge shapes as well as their influence on the ITD of a deformed ice field. Our high-resolution DEM simulations yield deformed ice covers with ridges of varying shapes, which we classify as triangular and trapezoidal ridges. Once classified, the influence of the trapezoidal ridges on the ITD becomes evident. Notably, the effect of varying ridge shapes on ITD has not been included into any ice redistribution scheme, even if ridges occur in nature with

https://doi.org/10.5194/egusphere-2025-6421
Preprint. Discussion started: 27 January 2026

varying shapes (Timco and Burden, 1997; Strub-Klein and Sudom, 2012). Consequently, the ITD stemming from our DEM simulations is different to ITDs created by commonly used sub-grid parametrizations in continuum models, namely both ridging functions developed by Hibler (1980) (HI80) and Lipscomb et al. (2007) (LI07). Further, we also demonstrate that the ITD yielding from DEM simulations also differ from those generated by continuum sea-ice models, here namely the neXt-generation Sea Ice Model (neXtSIM), where ice thickness within each grid cell is represented by its mean value only (Ólason et al., 2022). Thus, both conventional approaches representing ridges within continuum sea-ice models fail to represent ridges with a significant increase in ice thickness and their shape. These differences imply that only increasing the spatial resolution of continuum sea-ice models, within the limits of their practical application, is not sufficient to improve their skill in representing ridges as localized features within the ice cover. Further, we develop an analytical description of the distribution of ridged ice, which successfully incorporates the effect of ridge shapes, and discuss when and how the function introduced could be used in ridging schemes. On a more general level, our work demonstrates the potential of high-resolution sea-ice modeling using DEM and its complementary role relative to conventional large-scale sea-ice models.

In what follows, Section 2 first describes the general setup of our numerical experiments, followed by a description of HiDEM and neXtSIM models used and sea-ice redistribution model implemented to account for sub-grid parameterizations of ridging. Section 3 presents our results, including a general description of the deformed ice fields yielded by different approaches. This section further shows how to derive an analytical description for the distribution of ridged ice with a notion on ridge shapes. Section 4 first discusses the influence of ridge shapes to the ITD as well as the differences in the ITD observed from HiDEM to field observations and second how ridging processes connect to the ITD. This section also includes open questions regarding how to implement the derived distribution of ridged ice in redistribution schemes.

2 Methods

Figure 1 describes the simulation setup with the main parameters summarized by Table 1. The simulations mimicked displacement-driven bi-axial compression tests, with constant velocities prescribed on the boundaries with constant y. Motion across the boundaries at $x = 0$ km and $x = 6$ km was restricted to prevent ice from drifting out of the domain. The domain size, $6 \times 6\,\mathrm{km}^2$, was chosen large enough to fit several ridges while keeping the wall clock times for the simulations moderate. In addition, the chosen domain size was large enough to fit several grid cells of a high-resolution continuum sea-ice model.

All simulations start with a uniform ice thickness, but a non-uniform distribution of ice strength, as described below. The ice cover is then compressed over a period of two hours leading to average nominal strain of about 25 %. Simulations are conducted with three different initial ice thicknesses $h_i = 0.5\,\mathrm{m}$, $1.0\,\mathrm{m}$ and $2.0\,\mathrm{m}$. This h_i range spans from thin ice up to the maximum thickness reached through thermodynamic growth (Maykut and Untersteiner, 1971).

2.1 HiDEM

The Helsinki Discrete Element Model (HiDEM) describes the intact sea ice by using spherical particles connected by Euler-Bernoulli beams (Åström, 2006). The motion of the particles is described by Newton's laws, with external forces applied to

https://doi.org/10.5194/egusphere-2025-6421
Preprint. Discussion started: 27 January 2026

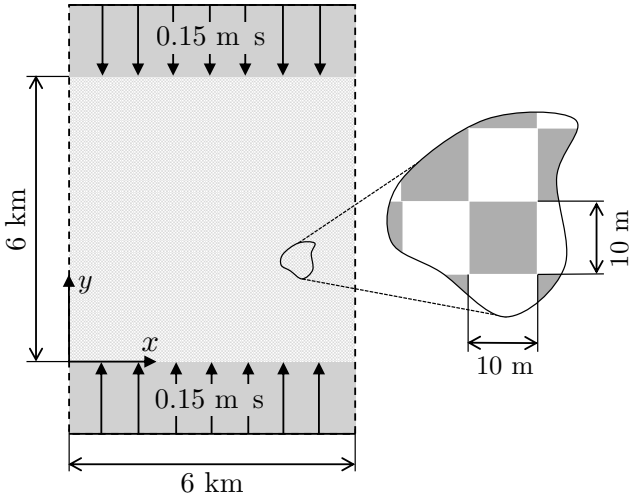

Figure 1. Description of the HiDEM simulation setup to also illustrate the overall simulation setup. The $6 \times 6\,\mathrm{km}^2$ observation area was split into a $10\,\mathrm{m} \times 10\,\mathrm{m}$ grid shown in the closeup to implement the inhomogeneity of the ice with each grid cell having a random beam probability between 0.4 and 1.0. A constant sea-ice velocity was applied so that level ice drifted into the observation area through the boundaries at $y = 0$ km and $y = 6$ km, while ice drift across the boundaries indicated by dashed lines at $x = 0$ km and $x = 6$ km was restricted.

them being due to elastic and inelastic contacts, buoyancy, gravity, drag, and friction. As the particles move, the beams deform. Upon reaching a predefined failure criterion, the beams fail, leading to ice failure and ice fragments of various sizes. More information on the version of HiDEM used can be found in Åström et al. (2024).

The simulated ice field was $6 \times 8.2\,\mathrm{km}^2$ and had the ice with $y < 0$ km and $y > 6$ km constrained to move in the y-direction with velocities of 0.15 m/s and -0.15 m/s, respectively (Figure 1). Thus, undeformed ice was pushed with constant velocity into the observation area of $6 \times 6\,\mathrm{km}^2$. We randomly removed beams bonding the particles to mimic the inhomogeneity of the ice cover and to create variation between the simulation runs with same h_i. This was done by splitting the ice initially within the observation area into a 10 m $\times$ 10 m grid, where each grid cell had its particle pairs linked by beams with a random probability between 0.4 and 1.0. Outside of the observation area, the beam probability was 0.8.

We conducted three simulations for $h_i = 2.0\,\mathrm{m}$, two for $h_i = 1.0\,\mathrm{m}$ and one for $h_i = 0.5\,\mathrm{m}$. The number of repeated simulations varied because we set the particle diameter equal to the ice thickness, meaning that the simulations with thinner ice required more particles than those with thick ice and, thus, came with higher computational cost. (The ice cover in the simulation with $h_i = 0.5\,\mathrm{m}$ had about $200 \cdot 10^6$ particles.) While the locations of the individual ridges showed variability between the runs with the same h_i, the resulting ITDs were practically identical. Nevertheless, the ITDs presented below are averaged across the simulations with same h_i. The output from the simulations was postprocessed into a gridded output with a resolution of $4h_i$ to describe the ice thickness (see Appendix A).

https://doi.org/10.5194/egusphere-2025-6421
Preprint. Discussion started: 27 January 2026

Table 1. Main parameters of the HiDEM and neXtSIM simulations.

General Setup	Value	Unit
Initial ice thickness h_i	0.5, 1.0, 2.0	m
Ice Velocity	0.15	ms^{-1}
Simulation time t	2	h
Observation area	6×6	km^2
neXtSIM		
Spatial resolution	100	m
Gridded spatial resolution	50	m
Temporal resolution	30	min
HiDEM		
Gridded spatial resolution	$4h_i$	m
Temporal resolution	10	min

2.2 neXtSIM

The neXt-generation Sea Ice Model (neXtSIM) was chosen as the continuum model, where the sea-ice cover is described with a brittle Bingham-Maxwell rheology on a triangular, Lagrangian grid (Ólason et al., 2022). According to the comparison of several high-resolution models, neXtSIM fulfills the requirements to reproduce realistic linear kinematic features, which are bands of high deformation and thus, can be related to ridging (Hutter et al., 2022). The sea-ice thickness, and changes due to deformation, are represented via a mean thickness. During the simulations, the standard stand-alone variables, as presented in Ólason et al. (2022), are used and the sea-ice thermodynamics are turned off.

To adapt neXtSIM to the idealized setup, ice gets generated at the boundaries, where the velocity is applied. Thus, throughout the whole simulation, ice with the initial ice thickness gets added into the simulation. To introduce variability between the simulations as well as a non-uniform ice strength, the cohesion is varied randomly in space between a maximum value and half of that maximum value. To account for variability, neXtSIM simulations are repeated five times.

Compared to the standard setting, the time step and resolution are significantly increased. The main model time step, controlling the advection, is 1 s, with 240 sub-cycles used to solve the dynamics yielding in a dynamical time step of $1/240 \approx 0.004\,\mathrm{s}$. The spatial resolution of the simulation was 100 m for the triangular Lagrangian grid, resulting in gridded output with a spatial resolution of 50 m.

2.3 Sea-ice redistribution model

To complement the results from neXtSIM, we also use a simple sea-ice redistribution model describing the sub-grid parametrization of ridging within continuum models utilizing an ice thickness distribution (ITD). Thus, the ITD is given by $g(h)$ separating

https://doi.org/10.5194/egusphere-2025-6421
Preprint. Discussion started: 27 January 2026

the ice within a grid cell in categories based on the ice thickness h and represents the amount of ice area and volume within each of these categories. Between each time step, the ice gets redistributed based on different redistribution schemes, consisting of a participation function and a ridging function.

Our sea-ice redistribution model is based on the implementation of the mechanical redistribution in ICEPACK (Hunke et al., 2024) and adapted to simulate sea-ice redistribution as a stand-alone model with two different ridging functions commonly implemented in large-scale sea-ice models. Thus, the ridging function is either based on Hibler (1980) (HI80), assuming a linear redistribution of ice based on the assumption of triangular ridges, or on Lipscomb et al. (2007) (LI07), assuming an exponential distribution of more smaller ridges compared to deeper ridges. Overall, the theory of the redistribution based on Thorndike et al. (1975) and Lipscomb et al. (2007) and explained in more detail in the Appendix B.

At the start of the simulation, all sea ice is within one ice category describing the initial thickness h_i as given in Table 1. During each time step, we add the theoretical amount of ice area Δ to the ice thickness distribution $g(h)$ into the category of h_i. After that, we call the redistribution function Ψ. To ridge the whole amount of Δ, we need to apply Ψ several times until the sum of $A(h)$ is again $6\,\mathrm{km} \times 6\,\mathrm{km}$, as the ice area within HiDEM and neXtSIM is constant due to confinement. If Ψ is only applied once, the resulting $A(h)$ is bigger than $6\,\mathrm{km} \times 6\,\mathrm{km}$ as the amount of ice participating in the deformation is calculated from $g(h)$ by the weighting function $b(h)$ (Appendix B, Equation B4) and the resulting $A(h)$ is also influenced by assumptions of the ridging functions. Additionally, our implementation assumes the ice concentration to be 100 % instead of calculating opening/closing rates as well as additional advection. We used regularly spaced ice categories with lower boundaries ranging from 0.0 to 20 m with a spacing of 0.5 m, which covers the range of observed sea-ice thickness in our simulations. We used the redistribution model with a time step of 5 min to calculate $g(h)$ after 2 h.

Both ridging functions, HI80 and LI07, contain tunable parameters. For HI80, the main tunable parameter is the empirical thickness H_*, which often ranges between 25, as used, for example, in ICEPACK, and 100, as proposed by Hibler (1980). H_* directly influences the maximum depth of ridges $2\sqrt{H_* h_i}$, which is the upper limit of the ridging function $\gamma(h_i, h)$. For LI07, e-folding scale of $\gamma(h_i, h)$ depends on the tunable parameter μ influencing the depth of ridges as well as the amount of smaller ridges present. For our initial simulations, H_* and μ are set according to the standard settings of ICEPACK (Hunke et al., 2024), $H_* = 25\,\mathrm{m}$ and $\mu = 3\,\mathrm{m}^{1/2}$, both representing ice of about the same strength (Lipscomb et al., 2007). Further, we conduct simulations where we vary H_* to 50 m and 100 m, to include the value Hibler (1980) proposed, and μ to $4\,\mathrm{m}^{1/2}$ and $6\,\mathrm{m}^{1/2}$, to include similar simulations with LI07.

3 Results and analysis

3.1 Comparison of model results

Figure 2 illustrates the final deformed ice covers and differing ridge patterns in HiDEM and neXtSIM simulations. The ridges in HiDEM are mainly perpendicular to the direction of compression, whereas neXtSIM yields a dominant X-shaped ridge pattern accompanied by smaller ridges, consistent with the Mohr-Coulomb failure criterion implemented within its rheology. Nevertheless, thoroughly investigating the difference in spatial distribution between both would need simulations with more

https://doi.org/10.5194/egusphere-2025-6421
Preprint. Discussion started: 27 January 2026

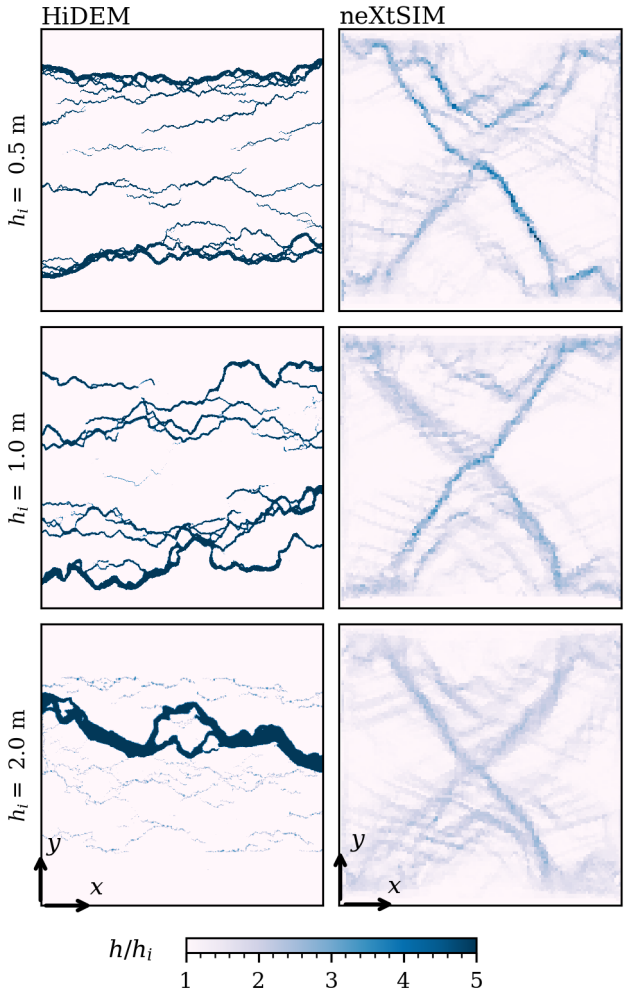

Figure 2. Ice thickness normalized by the initial thickness h_i for each h_i (0.5 m, 1 m and 2 m) and each model (HiDEM and neXtSIM) at the end of the simulations ($t = 2$ h). The domain size is $6 \times 6\,\mathrm{km}^2$. The arrows in the bottom left corner indicate the coordinate system, with the convergent velocity applied in y-direction.

diverse forcing scenarios and, thus, is a task for further studies. Omitting the distribution of ridges, both HiDEM and neXtSIM contain ridges as localized features embedded in an undeformed ice. The ridges in HiDEM are more strongly localized, while ridges in neXtSIM appear more smudged over several grid cells. Furthermore, the ridges are significantly shallower in neXtSIM than in HiDEM. Additionally, the number of ridges yielded by HiDEM increases with decreasing h_i.

To further investigate the ridges within HiDEM, we studied their cross-sectional shape. Therefore, we identified ridges with a thickness of $> 3h_i$ along five transects at $y = 1.0, 2.0, 3.0, 4.0$ and $5.0\,\mathrm{km}$ at the end of the simulation and manually classified

https://doi.org/10.5194/egusphere-2025-6421
Preprint. Discussion started: 27 January 2026

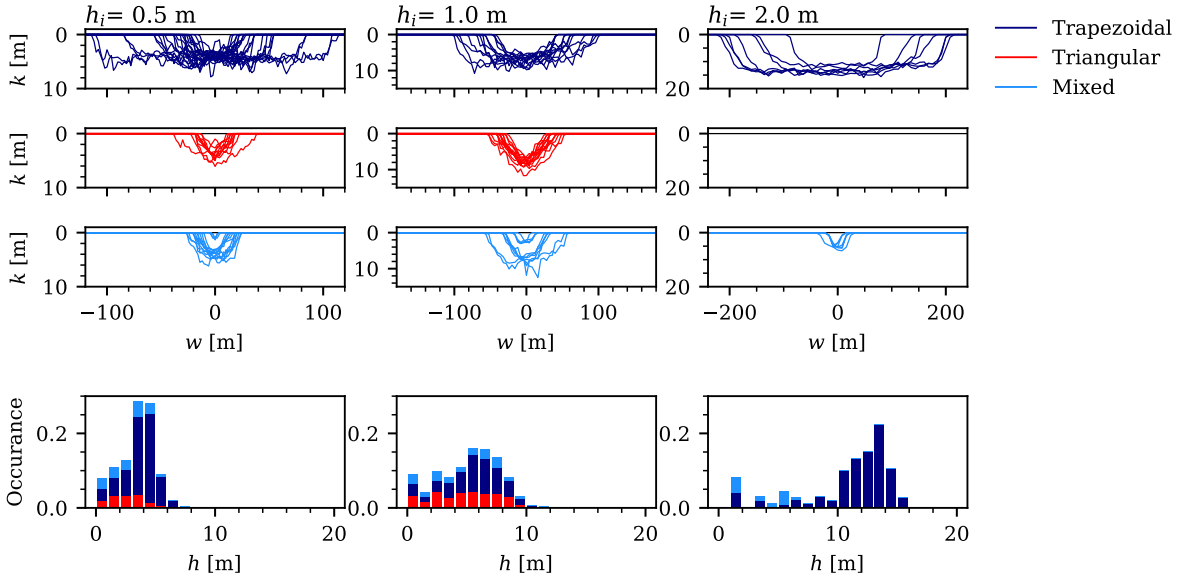

Figure 3. Ridge profiles are presented at the end of HiDEM simulations ($t = 2\,\mathrm{h}$) at five different cross-sections along the y-direction of the observation area for all h_i. The ridge profiles were manually classified into trapezoidal, triangular and mixed shape as indicated by the legend colors. The shape was only defined for ridges of depth $> 3h_i$. The histograms in the bottom row show the contribution of each ridge type to the distribution of deformed ice per ice thickness categories h. Here, the distribution of deformed ice is given regarding the relative area coverage of each h. Note, that the ranged of the axis for the ridge profile plots differs for each h_i.

the shape of their cross section into trapezoidal, triangular and mixed as Figure 3 shows. The mixed shape includes ridges very likely switching from triangular to trapezoidal shape as their shape is more round than triangular ridges, while not having an established plateau. The histograms in the bottom row of Figure 3 show how the ice within the ridges of each shape contributes to the area covered by each ice thickness, and thus to the volume. While most of the ridges stemming from ice of $h_i = 0.5\,\mathrm{m}$ and $1.0\,\mathrm{m}$ are triangular (46 % and 39 %, respectively), the trapezoidal ridges (22 % and 33 %, respectively) are large in size and consequently contribute more to the overall deformed ice both in area and volume. Similarly, for simulations with $h_i = 2.0\,\mathrm{m}$, about half of the ridges are rather large trapezoidal ridges, with the other half being small and of mixed shape; again, the trapezoidal ridges dominate the amount of deformed ice. Overall, the frequency of trapezoidal ridges increases with h_i.

Figure 4 shows the ice thickness distributions (ITD) calculated from the final deformed ice cover as presented in Figure 2. The ITD associated with HiDEM is bell curve-shaped, with its peak at ice thickness h, indicating the regime with the most of the deformed ice. This peak is around $h \approx 6h_i$, indicating a linear relationship between the h with most of the deformed ice volume and h_i. The histograms of Figure 3 indicate that this bump is connected to the ice in trapezoidal ridges, while the plateau between h_i and the start of the bump is influenced by the ice in the triangular ridges.

Figure 4 also presents the final ITD for neXtSIM as well as those calculated by the sea-ice redistribution models with HI80 and LI07 ridging functions. For both neXtSIM and LI07, the ITD features the largest amount of deformed ice close to h_i, with

https://doi.org/10.5194/egusphere-2025-6421
Preprint. Discussion started: 27 January 2026

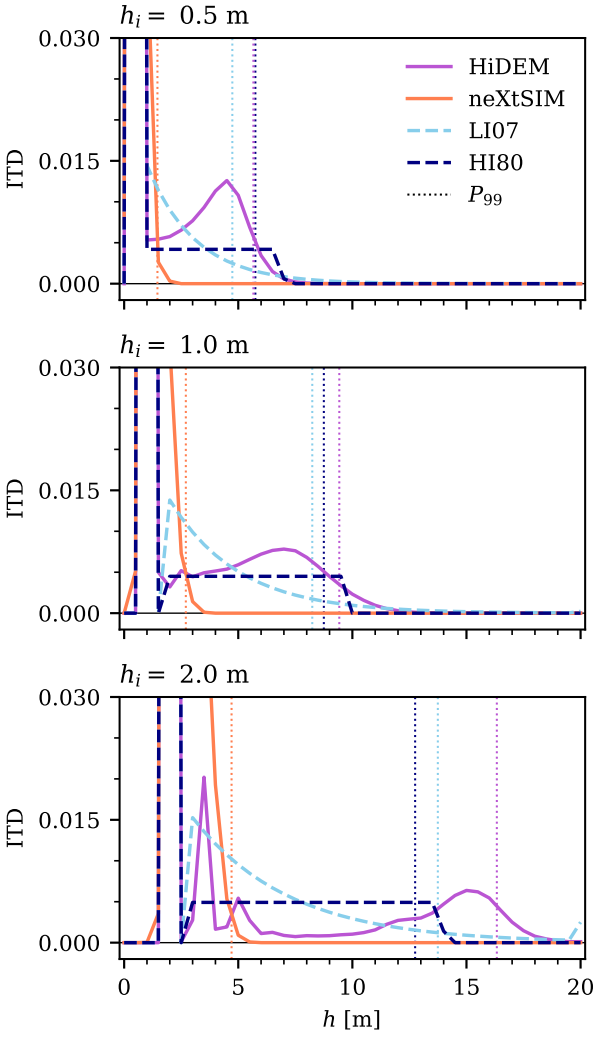

Figure 4. The ice thickness distribution (ITD) after $t = 2\,\mathrm{h}$ for HiDEM, neXtSIM and the results of the redistribution function utilizing two different ridging functions, LI07 and HI80 (Section 2.3). The dotted vertical line represents the upper 99^{th} percentile P_{99}. The ice categories are equally spaced categories form 0 to 20 m with a bin width of 0.5 m. The results of neXtSIM and HiDEM show the mean ITD and mean percentile across all simulations.

a gradual decrease towards thicker ice. This decrease is significantly faster for neXtSIM compared to LI07, with the upper 99^{th} percentile for neXtSIM being less than half of the 99^{th} percentile for LI07 (dotted lines in Figure 4). HI80 is, on the other hand, based on the assumption that the ridges are triangular, that the ice gets uniformly redistributed between the thickness of rafting and a set maximum ridge thickness (Appendix B). Consequently, the shape of the ITD is that of a flat line. Thus, neXtSIM and

https://doi.org/10.5194/egusphere-2025-6421
Preprint. Discussion started: 27 January 2026

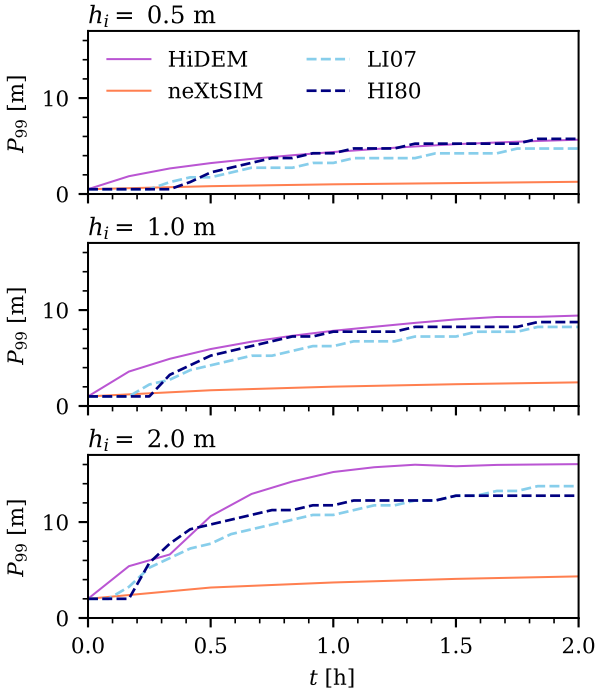

Figure 5. Development of the 99^{th} percentile is P_{99} of the ice thickness h within HiDEM, neXtSIM, LI07 and HI80 for each initial ice thickness h_i.

both redistribution functions, LI07 and HI80 create an ITD differing from that given by HiDEM resulting from both triangular and trapezoidal ridges.

Both HI80 and LI07 feature tunable parameters. As described in Section 2.3, we conducted sensitivity simulations within commonly used ranges of these parameters. For HI80, a lower H^* reduces the depth of ridges, and for, LI07 a smaller μ reduces the depth of ridges and results in more smaller ridges. Nevertheless, these tunable parameters do not influence the general shape of the ITD.

While the shape of the ITDs showed significant differences, the development of the upper 99^{th} percentile P_{99} of the ice thicknesses within the ITD align reasonably well between the sub-grid parametrizations and HiDEM simulations, as Figure 5 illustrates. The magnitude and development of P_{99} for HiDEM is nearly identical to that for HI80 and LI07 for $h_i = 0.5\,\text{m}$ and $1.0\,\text{m}$. For $h_i = 2.0\,\text{m}$, P_{99} for HiDEM simulated ice field is about $2h_i$ higher than P_{99} given by HI80 and LI07. Additionally, the development of HiDEMs P_{99} shows a plateau, resulting from the increase in width of the trapezoidal ridges, which had an approximately equal depth (Figure 3). Simultaneously, Figure 3 also shows that neXtSIM significantly underestimates the depth of deformed ice. Thus, the comparison of P_{99} demonstrated that including a sub-grid parametrization of ridging benefits the representation of deformed ice compared to a two-level approach which only includes the mean ice thickness, as shown by neXtSIM.

https://doi.org/10.5194/egusphere-2025-6421
Preprint. Discussion started: 27 January 2026

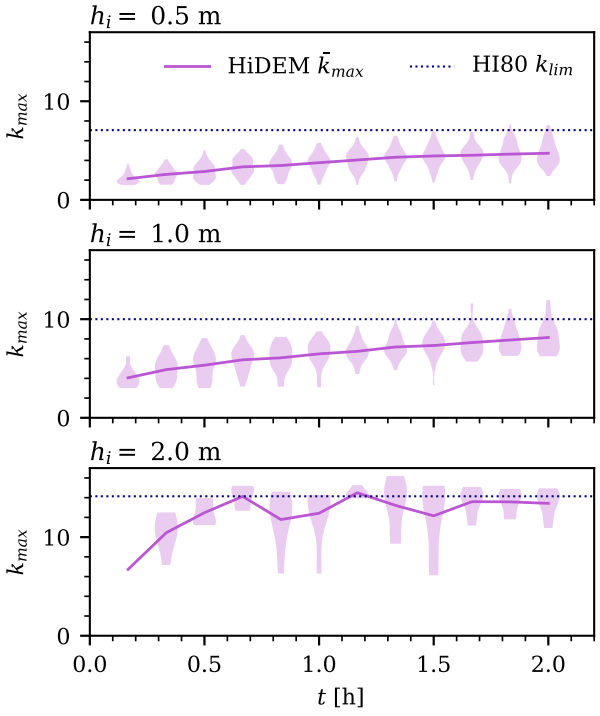

Figure 6. Evolution of the distribution of maximum keep depths k_{max} within HiDEM given as a violin plot for each time step for all three initial thicknesses h_i. Therefore, ridges were identified along five different cross sections along the x-direction of the observation area, if $k_{max} \geq 3h_i$. The mean of k_{max}, $\bar{k}_{max}$, is given as solid line. The upper limi of the keel depths k_{lim}, as calculated by Hibler (1980) (HI80), is given as a dotted constant blue line.

3.2 Distribution of ridged ice $n(h)$

Here, we introduce a new function describing the distribution of ridged ice $n(h)$, based on the influence of the ridge shape on the ITD (Figure 3). Conceptually, this function accounts for triangular ridges, similar to Hibler (1980), but extends it to include trapezoidal ridges. Thus, one input parameter of $n(h)$ is based on the maximum depth of ridges k_{max}. Figure 6 presents the evolution of the distribution of k_{max} in HiDEM as well as the mean of k_{max} given as $\bar{k}_{max}$. At $t = 2\,\mathrm{h}$, $\bar{k}_{max}$ is approximately constant for $h_i = 0.5\,\mathrm{m}$ and $h_i = 2.0\,\mathrm{m}$ and the distribution of k_{max} seems to only show minor changes for $h_i = 1.0\,\mathrm{m}$. To simplify this derivation, we treated the entire simulation time $t = 2\,\mathrm{h}$ as a single time step, which allowed us to treat $\bar{k}_{max}$ as a constant.

First, we propose splitting the ITD $g(h) = d(h) + u(h)$ with an ITD for deformed ice $d(h)$ and undeformed $u(h)$, meaning thermodynamically grown ice. Thus, during redistribution ice will be removed from $u(h)$ and added to $d(h)$ based on the newly calculated $n(h)$. This split has already proven to be useful to analyze sub-grid processes by Flato and Hibler (1995), as $d(h)$ offers detailed information on the properties of the ridges within one grid cell.

https://doi.org/10.5194/egusphere-2025-6421
Preprint. Discussion started: 27 January 2026

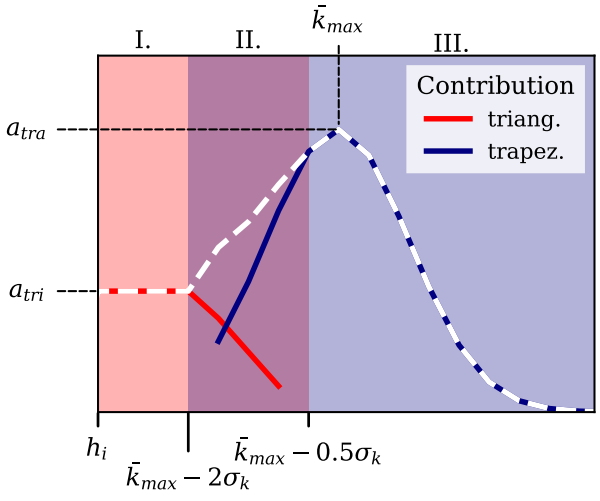

Figure 7. Sketch illustrating the the derivation of the distribution of ridged ice $n(h)$ including the contribution of the triangular and trapezoidal ridges in red and blue shading, respectively. $n(h)$ contains of three parts: Part I is influenced by triangular ridges only and Part III by trapezoidal ones, while Part II describes the transition between them. All input parameters of $n(h)$ are annotated as well: a_{tri}, a_{tra}, $\bar{k}_{max}$ and σ_k.

To describe the ridged ice $n(h)$, the function is split into three different parts describing different ridge shapes as illustrated in Figure 7. First, the plateau of Part I, having a value a_{tri}, describes the contribution of triangular ridges. Part III describes the trapezoidal ridges using a Gaussian curve with the maximum value a_{tra}. Part II describes the transition between the two and comprises of a linear function decreasing from a_{tri} to zero, as well as the same Gaussian curve as Part III. Thus,

$$n(h) = \begin{cases} a_{tri}, & \text{Part I} \\ a_{tri}\left(1 + \frac{\bar{k}_{max} - 2\sigma_k}{1.5\sigma_k}\right) - \frac{a_{tri}}{1.5\sigma_k}h + & \text{Part II} \\ \quad a_{tra}\exp(-\frac{(h-\bar{k}_{max})^2}{2\sigma_k^2}), & \\ a_{tra}\exp(-\frac{(h-\bar{k}_{max})^2}{2\sigma_k^2}), & \text{Part III} \end{cases} \tag{1}$$

where σ_k is the standard deviation of k_{max}. Part I is calculated for h between $h_i \leq h < \bar{k}_{max} - 2\sigma$. The upper boundary of Part I also defines the lower boundary of the Gaussian function influencing Parts II and III. Thus, this boundary is set so that most of the Gaussian function is included in $n(h)$, as everything above the lower $2\sigma_k$ limit accounts for around 97 % of a normal distribution. Part II is then calculated between $\bar{k}_{max} - 2\sigma \leq h < \bar{k}_{max} - 0.5\sigma$, where the upper boundary was chosen ad hoc so that the transition between Part I and Part III is smooth. The factors in front of σ_k in Equation 1 are a consequence of integration between those boundaries. Here, we calculate $n(h)$ first based on the sea-ice area $n_A(h)$ and then calculate the distribution of ridged ice for the volume as $n_V(h) = n_A(h)h$ as continuum models typically feature $g(h)$ both for the sea-ice area and volume.

https://doi.org/10.5194/egusphere-2025-6421
Preprint. Discussion started: 27 January 2026

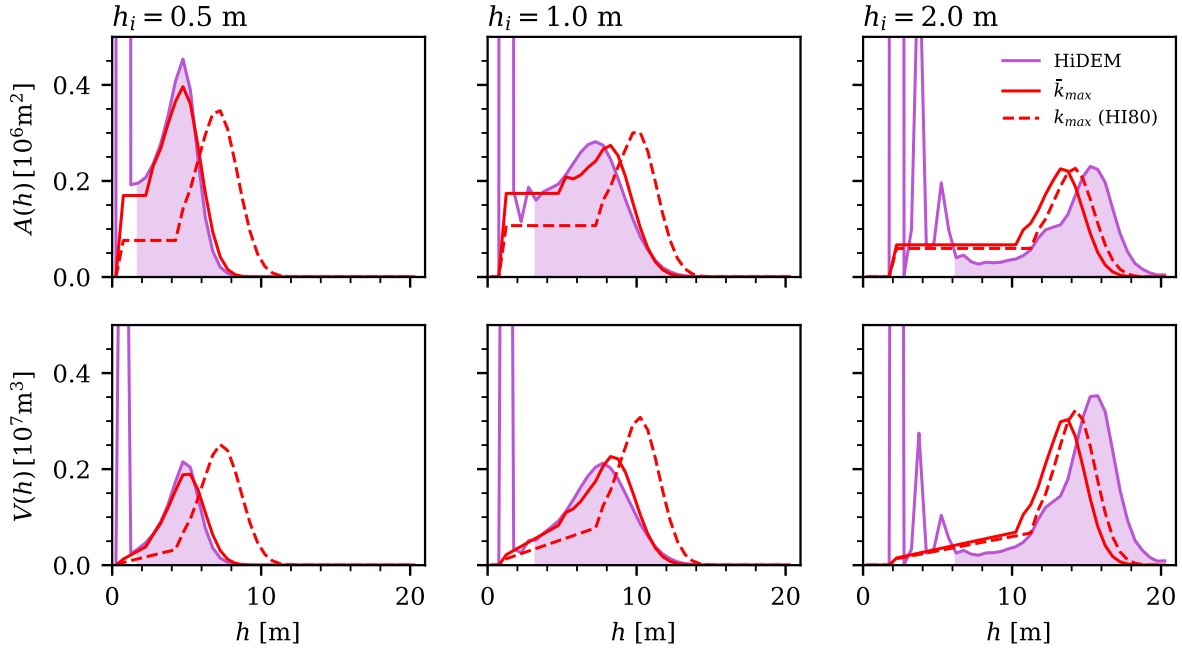

Figure 8. Results of the distribution of ridged ice $n(h)$ (Equation 1) compared against the HiDEMs ITD after t =2 h, with the deformed ice $d(h)$ being highlighted by the shading for $3h_i \leq h$. $n(h)$ was calculated either with $\bar{k}_{max}$ and σ_k calculated based on HiDEM data (solid line) or with $\bar{k}_{max}$ based on Hibler (1979) and σ_k being a mean value (dashed line).

To calculate Equation 1, we rely on the ITD describing the distribution of the deformed-ice area $d_A(h)$. From $d_A(h)$, we calculate the sum of deformed area A_d from $\sum_h d(h)$ as the area under $n_A(h)$ must be equal to A_d. Additionally, we define that $\alpha = A_{tri}/A_{tra}$, where α is a tuning parameter, and thus $A_d = A_{tri}(1+1/\alpha)$. Overall, α regulates the relationship between
225 triangular to trapezoidal ridges, and thus, a higher α results in a more pronounced "bump", signaling more trapezoidal ridges. Nevertheless, $\alpha > 0$, as also trapezoidal ridges contribute to the plateau of $n(h)$. Then, a_{tri} can be calculated based on A_{tri}, calculated based on the integral over the constant part of $n_A(h)$ and the decreasing linear function:

$$A_d = a_{tri}\left(\bar{k}_{max} - h_{ini} - 1.25\sigma_k\right)\left(1 + \frac{1}{\alpha}\right). \tag{2}$$

To calculate a_{tra}, we calculate A_{tra} based on the integral of an arbitrary Gaussian function being $\int_{-\infty}^{\infty} \exp\left(-1(x+b)^2\right) dx =$
230 $\sqrt{\pi/a}$. Including α, a_{tra} can be calculated based on a_{tri}:

$$a_{tra} = \frac{a_{tri}}{\alpha}\left(\frac{\bar{k}_{max} - h_{ini} - 1.25\sigma_k}{\sigma_k\sqrt{2\pi}}\right). \tag{3}$$

Apart from the tuning parameter α, the input parameters of $n_A(h)$ depend on A_d, which is known during the simulation, and $\bar{k}_{max}$ and σ_k, which could also be derived from ridge observations.

https://doi.org/10.5194/egusphere-2025-6421
Preprint. Discussion started: 27 January 2026

We used two approaches to estimate $\bar{k}_{max}$ and σ_k. First, we estimate $\bar{k}_{max}$ and σ_k from HiDEM data. Therefore, we sample k_{max} for each ridge with $k_{max} \geq 4h_i$ to exclude small and underdeveloped ridges at $t = 2\,\mathrm{h}$. The mean and standard deviation of this dataset corresponds to $\bar{k}_{max}$, as shown in Figure 6, and σ_k, respectively. While $\bar{k}_{max}$ increases with h_i (4.7 m, 8.1 m and 13.4 m for h_i = 0.5, 1.0 and 2.0 m), the values for σ_k are relatively similar to each other (1.2 m, 1.5 m and 1.4 m for h_i = 0.5, 1.0 and 2.0 m). Second, we calculate $\bar{k}_{max}$ based on the upper limit for the HI80 redistribution $k_{lim} = 2\sqrt{H_* h_i}$ with $H_* = 25$, shown as the blue dotted line in Figure 6, and use the mean of σ_k from HiDEM data. The tuning parameter α was chosen ad hoc ($\alpha = 0.25, 0.55$ and 0.5 for $h_i = 0.5, 1.0$ and 2.0 m, respectively). Thus, both versions of the redistribution of ridged ice $n_A(h)$ and $n_V(h)$ are shown together with $g_A(h)$ and $g_V(h)$ yielded by HiDEM in Figure 8.

Overall, the shape of $n(h)$ is consistent with the results from HiDEM. Estimating $\bar{k}_{max}$ and σ_k from HiDEM results in a closer fit than using the HI80 approach. The different phases of $n(h)$ (Equation 1) successfully reproduce the plateau towards thinner ice as well as the bump towards thicker ice. Estimations of $\bar{k}_{max}$ based on HiDEM data only show very small differences in the location of the peak in $g(h)$ for h_i =0.5 m and 1.0 m, calculated from the whole observation area. For $h_i = 2.0\,\mathrm{m}$, $\bar{k}_{max}$ is 1.83 m smaller than the location of the peak, as the distribution skews slightly towards smaller k_{max}, indicating that the median of k_{max} could have been the more appropriate value for constructing Equation 1 (Figure 6).

Additionally, calculating $\bar{k}_{max}$ based on k_{lim} (HI80) overestimates the location of the peak, and thus the thick ice, for $h_i = 0.5\,\mathrm{m}$ and 1.0 m, highlighting that this calculation method might not be suitable for estimating $\bar{k}_{max}$ (Figure 8). Contrary to k_{max} based on HI80, $\bar{k}_{max}$ derived from HiDEM seems to follow a linear relationship with h_i at $t = 2\,\mathrm{h}$. It should be noted that k_{lim} was derived to estimate the overall upper limit of the distribution and not a mean distribution of maximum keel depths. Thus, while the derived function to describe ridged ice $n(h)$ captures the ITD from HiDEM, for larger-scale applications, it is important to select the input variables carefully.

4 Discussion

4.1 Ridge shapes and ITD

Field observations have shown, that the shapes of ridges show large variability with a triangular shapes often assumed for first-year ridges and a trapezoidal shapes for multi-year ridges (Timco and Burden, 1997; Strub-Klein and Sudom, 2012). We also observe variety of shapes and dimensions of the ridges yielding from HiDEM simulations, demonstrating the strength of DEM in explicitly resolving ice failure and ridging processes (Figure 3). Ridges in HiDEM appear as clearly localized with a significantly increased thickness compared to the surrounding, undeformed ice (Figure 2).

Number of ridges within our 6 km × 6 km domain decreased with increasing h_i in our HiDEM simulations (Figure 2). This observation is intuitive, as the characteristic length, $L_C \propto h^{3/4}$, for a beam or plate on an elastic foundation (Hetenyi, 1946). L_C is related to the failure length of such a beam or plate under bending; for a given area of ice cover, thin ice is expected to fail more frequently than thick ice. L_C is often used to assess the length scale for ice failure (Sanderson, 1988; Hopkins, 1998; Amundrud et al., 2004). Analogously, field observations analyzed by Uusinoka et al. (2025a) suggest that thin

https://doi.org/10.5194/egusphere-2025-6421
Preprint. Discussion started: 27 January 2026

ice yields spatially more frequent deformation features than thick ice, whereas the deformation features with thick ice are more prominent. Both of these observations align with those related to the ridging in HiDEM simulations.

Commonly used ridging functions do not capture the ITD of the deformed ice cover produced by HiDEM (Figure 4). This discrepancy is due to the ridges of trapezoidal shape, which yield a bump in the ITD around the thickness h representing the keel depth. Previous two-dimensional DEM simulations on the formation of individual ridges similarly yielded trapezoidal ridge shapes that had a similar effect on the ITD (Hopkins, 1996, 1998). Our findings, importantly, extend these results by confirming that trapezoidal ridges have a significant effect on the ITD for a deformed ice cover, which contain multiple ridges. While the relative number of trapezoidal ridges increases with h_i, their influence on the ITD is significant for the thinnest ice tested here as well. Thus, even with the ice cover thinning due to climate warming and simultaneously the number of ridging events increasing (Krumpen et al., 2025), ridging schemes should account for various ridge shapes.

ITDs are generally formulated based on observations on the distribution of ridge keels (Melling and Riedel, 1996; Amundrud et al., 2004; Yu et al., 2004; Metzger et al., 2021), the distribution of sails via surface elevation (Petty et al., 2016), via electromagnetic measurements of the whole ice thickness (Haas et al., 2009) or by using a combination of these methods (Haas et al., 2008). These studies led to ITDs with a long tail representing ridges, which is often described by a negative exponential function (Amundrud et al., 2004; von Albedyll et al., 2021). This differs from the shape of the ITDs here. All of the aforementioned observations are conducted over larger areas with more variations in the ice conditions, for example thickness and ice motion, than the here used observation area. Additionally, they reflect ice deformation that has occurred in multiple stages over longer periods. Hopkins (1996) suggested that the negative exponential form stems from thickness contributions of multiple ridges in various stages of development superposed; the negative exponential form may consist of several bumps combined into one curve. In von Albedyll et al. (2021), an ITD calculated over fast ice contains a bump between 3.0 m and 3.5 m and a bump around 2.5 m with a plateau leading up to it. Assuming that fast ice has a more uniform thermodynamically-grown thickness, this observation supports our observation of an ITD containing a bump to describe ridges.

To date, the only link between ridge shapes to negative-exponential tail of the ITD is based on the assumption that an average ridge has a cusp shape (Amundrud et al., 2004). This average ridge shape has been observed by Metzger et al. (2021) analyzing underwater keel measurements. They argue, that the cusp shape is a result of shearing. The assumption on such shape contradicts current understanding of how ridges form as demonstrated by direct field observations and numerical simulations.

4.2 Ridging processes and ITD

The derivation of the proposed distribution of ridged ice $n(h)$ (Equation 1) leaves two main questions to be addressed for its implementation into a continuum sea-ice model: (1) how do $\bar{k}_{max}$, σ_k and α depend on the deformation history of a grid cell or can they be assumed constant and (2) what is the process scale to calculate volume of deformed ice V_d? Once these questions are answered, $n(h)$ could replace the ridging function $\gamma(h_i, h)$ in redistribution schemes. Overall, they relate to open questions regarding the understanding of ridging processes and are explored next.

Current ridging functions, like that of H80, assume a global limit for the ridge depth, k_{lim}, and ignore a potential development of the maximum depth of each ridge k_{max} during deformation. While we observe variation between the individual ridge depths

https://doi.org/10.5194/egusphere-2025-6421
Preprint. Discussion started: 27 January 2026

yielded by HiDEM, the mean of the maximum keel depths $\bar{k}_{max}$ reaches a constant value, as the ridges start growing in width and transfer towards trapezoidal shape (Figures 3 and 6). Additionally, σ_k shows no significant variation with h_i and can be assumed constant. Thus, we propose using a $\bar{k}_{max}$ that increases linearly with h_i. Nevertheless, a more sophisticated implementation of $\bar{k}_{max}$ could depend on the available forcing during a deformation event, as proposed by a folding rate of the ITD proportional to the deformation rate (von Albedyll et al., 2021) and the available ice (Amundrud et al., 2004).

Most observations have focused on finding k_{lim} instead of distribution of k_{max} via $\bar{k}_{max}$ and σ_k. Thus, using $\bar{k}_{max}$ instead of k_{lim} within our ridging function accounts for the fact that several ridges may not reach k_{lim}, due to either the surrounding ice thermodynamically having thickened since the ridge building, the keel melting, or all available ice having been incorporated into the ridge (Amundrud et al., 2004). Based on observations, Amundrud et al. (2004) found a k_{lim} of $20\sqrt{h_i}$ with is equal to Hibler (1980) with a $H^* = 100$. This limit is significantly higher than the HI80 k_{lim} calculated with $H^* = 25$, as used in this study and in ICEPACK. Further, HI80 k_{lim} is a close upper bound to the observed distribution of k_{max} in HiDEM (Figure 6).

Deriving a relationship for α depends on, for example, the number of ridges in a grid cell or the severity of ice deformation. Our results suggest that a relationship for α must account for the ice thickness, but α could also be connected to the large-scale ice strength or to the severity of deformations. Values or functions for α could be determined by comparing results from a sea-ice model utilizing the suggested scheme with observations or by using results from DEM simulations with diverse forcing scenarios and varying initial ITDs.

The calculation period of the volume of deformed ice V_d needs to have a defined start and end point within the redistribution scheme. Deformation events, and thus ridging, seem to have a temporal scale of several hours (von Albedyll et al., 2022), which would indicate calculating V_d over the scale of a deformation event. Instead of using the length of a deformation event as the period over which V_d accumulates, the period may also be limited by the consolidation time of the formed ridges, as the initial consolidation occurs over a period varying from hours to days, depending on the initial ice thickness and surrounding conditions (Maus, 2025). Therefore, for example, the model developed by Salganik et al. (2020) could be used. However, it is unclear whether ridges grow only during a single deformation event or whether subsequent events continue to grow the same ridges rather than establish new ones.

The following examples highlight how the implementation of $n(h)$ and its requirements may benefit other areas of sea-ice dynamics within continuum sea-ice models. First, the split of $g(h)$ into $d(h)$ and $u(h)$ consequently requires a reformulation of the participation function $a(h)$ (Equation B3 in Appendix B) to only allow undeformed ice to get deformed, $a(h) = b(h)u(h)$. This reformulation improves the physical meaning of the function, as it accounts for ridges only consisting of broken-off ice blocks from the surrounding level ice (Strub-Klein and Sudom, 2012; Kulyakhtin and Høyland, 2014). Second, having a separate distribution for deformed ice via $d(h)$ allows us to account for macroporosity in ridges, with, for example, either a mean macroporosity or parameterizations like the one proposed by Maus (2025). Currently, redistribution functions do not account for macroporosity within ridges, except for the scheme proposed in Roberts et al. (2019). Third, ridge-grounding schemes could be directly connected to results from redistribution, as Dupont et al. (2022) argued that high fractions of likely undeformed thin ice within $g(h)$ influenced their calculation of the maximum keel depth and thus the grounding of ridges. These ridges are important for the representation of land fast ice (e.g. Mahoney et al., 2007).

https://doi.org/10.5194/egusphere-2025-6421
Preprint. Discussion started: 27 January 2026

With the split of $g(h)$, it is possible to create ice categories suitable for both thermodynamics and redistribution of ice. Currently used ranges better resolve thinner ice with, for example, the lower bounds of the ice categories for ICEPACK (original setting) are 0, 0.64, 1.39, 2.47, and 4.57 m (Hunke et al., 2024). These ranges highlight that current implementations of the ITD focus on the representation of thin ice, as it has a stronger effect on thermodynamics, whereas a significant fraction of ridged ice falls within a single ice category.

Overall, the spatial comparison of HiDEM and neXtSIM and the comparison of the ITDs yielded by them implies that only increasing the spatial resolution of continuum models, within the limits of their practical use, is not sufficient to improve the representation of ridges as localized features within the ice cover. This observation aligns with results from a comparative study by Hutter et al. (2022). In their case, the limit was related to the tendency of high-resolution continuum simulations to produce leads rather than ridges. Further limits to the applicability of continuum models in high-resolution modeling are set by the minimum domain size for observing scale invariance and multifractal behavior of sea ice (Uusinoka et al., 2025a, b). Thus, representing ridging even in high-resolution continuum models will require suitable sub-grid parametrizations of ridging as well as the connection of ridging to the large-scale ice strength. To this end, as also demonstrated here, DEM models are a suitable tool to complement continuum models in detailed investigations on sea-ice deformation.

5 Conclusions

We conducted high-resolution simulations to study how the ridge shape influences the ice thickness distribution (ITD) by using a three-dimensional discrete element model, HiDEM, which enabled us to simulate ice failure and ridge-formation processes explicitly. Further, we compared these results to those from neXtSIM, a continuum model representing the ice thickness by the mean thickness, and to two commonly employed redistribution schemes in sea-ice models using ITD, with the ridging function based on Hibler (1980) (HI80) and Lipscomb et al. (2007) (LI07). From our results and discussions, we can summarize the following conclusions:

- The ITD from the DEM simulations shows a significantly different shape compared to the ITD from the other three models, because HiDEM forms trapezoidal-shaped ridges, which the others do not (Figure 4). The trapezoidal-shaped ridges cause a pronounced bump towards the thicker ice categories (Figure 4).
- Implementing an ITD with a sub-grid parametrization of ridging seems to be beneficial for the representation of thick ice, as shown by the comparison of ITDs stemming from neXtSIM, using a mean thickness, and the redistribution schemes (HI80 and LI07) (Figure 5).
- We present an analytical redistribution function that captures the triangular and trapezoidal ridge shapes. The main parameters in this function are the mean maximum keel depth and its standard deviation, and a tuning parameter governing the fraction of trapezoidal to triangular ridges (Equation 1 and Figure 8).

While the discrete-element-method simulations in this paper described a fairly simple deformation scenario, they still yield a deformed ice field with diverse of ridge shapes and sizes. Thus, an interesting next steps would be to study the effects of more

https://doi.org/10.5194/egusphere-2025-6421
Preprint. Discussion started: 27 January 2026

complex forcing, to investigate ITDs related to shear-ridge formation, or start the simulations with an already deformed and partially healed ice cover.

Code and data availability. The HiDEM code used here is a beta-version and not yet publicly available, while an older released version of the code is available at Todd (2018). neXtSIM is available at https://github.com/nansencenter/nextsim, while the exact version used for these experiments is archived at https://doi.org/10.5281/zenodo.17974261. The implementation of the sea-ice redistribution model and the analytical function and the simulation results can be requested from Marek Muchow.

Appendix A: Processing of HiDEM data

The standard simulation output of HiDEM contains information on a particle level, which needs to be transformed into gridded data to be comparable between HiDEM simulations and with neXtSIM. Particle level means, that at every output timestep we know the location of each individual particle, but, for example, not the extent of a ridge consisting of several particles.

The gridded HiDEM data contains the ice thickness h as well as keel depth and sail height. To create the gridded data, the simulation domain is divided into a regular grid with the spacing dx depending on the initial ice thickness h_i, being the diameter of each particle, $dx = 4h_i$. The ice thickness within each grid cell is calculated based on the minimum and maximum location of the centroid of each particle: $h = z_{max} + 0.5h_i - z_{min} - 0.5h_i$. Similarly, the keel depth and sail height are calculated, but with respect to the water level. Here, these calculations result in gridded data with a spatial resolution of $2\,\mathrm{m}$ to $8\,\mathrm{m}$.

It is important to note, that the ice thickness calculated in areas with deformation contains the void space, macroporosity, between ice blocks in the ridges. This characteristic makes HiDEM the only model in this study to consider macroporosity, compared to neXtSIM and both redistribution models.

Appendix B: Sea-ice redistribution theory

Originally, the sea-ice redistribution was introduced by Thorndike et al. (1975) and then further developed by Lipscomb et al. (2007) to enhance model stability and improve agreement between modeled and observed ice thickness distributions.

In our case, the redistribution function Ψ only needs to be applicable for convergence. Thus, it can be described by the ridging mode w_r and the strain rate magnitude $|\dot{\epsilon}|$:

$$\Psi = w_r(h, g)|\dot{\epsilon}|. \tag{B1}$$

Similar to von Albedyll et al. (2022), we use the area change Δ as a proxy for $|\dot{\epsilon}|$ as we know how much area is added per time step dt to the system ($\Delta = 2Lvdt$ with L the length of the observation area in y-direction and v the ice velocity) and thus, needs to ridge to be comparable to the other simulations.

https://doi.org/10.5194/egusphere-2025-6421
Preprint. Discussion started: 27 January 2026

The ridging mode w_r is a function of the participation function $a(h)$, describing which ice gets ridged per thickness category h, and the distribution of ridged ice $n(h)$, and can be written as:

$$w_r = \frac{-a(h) + n(h)}{N} \tag{B2}$$

N serves as a normalization factor for area conversation. The participation function is thus a function of $g(h)$, the original ITD:

$$a(h) = b(h)g(h). \tag{B3}$$

Here, we use the weighing function $b(h)$ introduced by Lipscomb et al. (2007), which is a smooth approximation of $b(h)$ originally formulated by Thorndike et al. (1975).

$$b(h) = \frac{e^{G(h)/a^*}}{a^* \cdot (1 - e^{-1/a^*})} \tag{B4}$$

with the empirical parameter $a^* = 0.05$ and the cumulative thickness distribution function $G(h)$. Thus, $b(h)$ allows all ice to participate in ridging, but favors the thin ice present. We only use one participation function, as the focus of this study lies on ridging.

Additionally, $n(h)$ depends on $a(h)$ and the ridging function $\gamma(h_i, h)$

$$n(h) = \int_0^\infty a(h_i)\gamma(h_i, h)dh_i, \tag{B5}$$

where h_i describes the initial thickness before ridging.

For $\gamma(h_i, h)$ we implemented two different functions, which each are based on different redistribution approaches. Based on the geometrical assumption, that the cross-section of a ridge is roughly triangular, Hibler (1980) (HI80) proposed a uniform distribution:

$$\gamma(h_i, h) = \begin{cases} \frac{1}{2(H_* - h_i)}, & 2h_i \leq h \leq 2\sqrt{H_* h_i} \\ 0, & \text{otherwise} \end{cases} \tag{B6}$$

with the empirical thickness H_*. Thus, redistribution is only allowed between $2h_i$ (rafting) and a limit depth for ridges $k_{lim} = 2\sqrt{H_* h_i}$. Later, Lipscomb et al. (2007) (LI07) developed an exponential function of γ

$$\gamma(h_i, h) = \begin{cases} \gamma_0 e^{\frac{-(h - h_{min})}{\mu\sqrt{h_i}}}, & h \geq h_{min} \\ 0, & \text{otherwise} \end{cases} \tag{B7}$$

with γ_0 being a normalization factor and μ a tunable parameter influencing the folding scale. The minimum thickness of ice participating in ridging h_{min} is defined as $h_{min} = \min(2h_i, h_i + h_{\text{raft}})$ with h_{raft} being 1 m.

https://doi.org/10.5194/egusphere-2025-6421
Preprint. Discussion started: 27 January 2026

Author contributions. MM, EÓ and AP conceptualized the study. EÓ adapted the neXtSIM to the study setup and MM created the HiDEM setup. MM conducted all simulations, analyzed the results, derived the analytical function and wrote the paper. EÓ and AP contributed to the analysis and writing of the paper.

Competing interests. The authors declare that they have no conflict of interest.

Acknowledgements. MM is grateful for the funding from the AaltoENG 4-year doctoral program and acknowledges the funding from the European Union—NextGenerationEU instrument through Research Council of Finland under Grant (348586) WindySea–Modelling engine to design, assess environmental impacts, and operate wind farms for ice-covered waters. In addition, MM acknowledges the Finnish Maritime Foundation (Merenkulun Säätiö) for funding the research stay at the Nansen Center. EÓ was supported by the MuSIC project, funded by the Norwegian Research Council (no. 325292) and internal funds from the Nansen Center. AP is grateful for financial support from the Research Council of Finland through the project (347802) DEMFLO: Discrete Element Modeling of Continuous Ice Floes and Their Interaction. The authors wish to acknowledge the CSC – IT Center for Science (Finland) – for computational resources.

https://doi.org/10.5194/egusphere-2025-6421
Preprint. Discussion started: 27 January 2026

References

Amundrud, T. L., Melling, H., and Ingram, R. G.: Geometrical Constraints on the Evolution of Ridged Sea Ice, Journal of Geophysical Research: Oceans (1978–2012), 109, https://doi.org/10.1029/2003jc002251, 2004.

Åström, J. and Polojärvi, A.: High-Resolution Fracture Dynamics Simulation of Pack-Ice and Drift-Ice Formation During Sea Ice Break up Events Using the HiDEM2.0 Code, Geophysical Research Letters, 51, e2024GL110 552, https://doi.org/10.1029/2024GL110552, 2024.

Åström, J., Robertsen, F., Haapala, J., Polojärvi, A., Uiboupin, R., and Maljutenko, I.: A Large-Scale High-Resolution Numerical Model for Sea-Ice Fragmentation Dynamics, The Cryosphere, 18, 2429–2442, https://doi.org/10.5194/tc-18-2429-2024, 2024.

Åström, J. A.: Statistical Models of Brittle Fragmentation, Advances in Physics, 55, 247–278, https://doi.org/10.1080/00018730600731907, 2006.

Blockley, E., Vancoppenolle, M., Hunke, E., Bitz, C., Feltham, D., Lemieux, J.-F., Losch, M., Maisonnave, E., Notz, D., Rampal, P., Tietsche, S., Tremblay, B., Turner, A., Massonnet, F., Ólason, E., Roberts, A., Aksenov, Y., Fichefet, T., Garric, G., Iovino, D., Madec, G., Rousset, C., y Melia, D. S., and Schroeder, D.: The Future of Sea Ice Modelling: Where Do We Go from Here? The Future of Sea Ice Modelling: Where Do We Go from Here?, Bulletin of the American Meteorological Society, 101, E1304–E1311, https://doi.org/10.1175/bams-d-20-0073.1, 2020.

Bouchat, A., Hutter, N., Chanut, J., Dupont, F., Dukhovskoy, D., Garric, G., Lee, Y. J., Lemieux, J.-F., Lique, C., Losch, M., Maslowski, W., Myers, P. G., Ólason, E., Rampal, P., Rasmussen, T., Talandier, C., Tremblay, B., and Wang, Q.: Sea Ice Rheology Experiment (SIREx): 1. Scaling and Statistical Properties of Sea-Ice Deformation Fields, Journal of Geophysical Research: Oceans, 127, https://doi.org/10.1029/2021jc017667, 2022.

Brenner, S., Rainville, L., Thomson, J., Cole, S., and Lee, C.: Comparing Observations and Parameterizations of Ice-Ocean Drag Through an Annual Cycle Across the Beaufort Sea, Journal of Geophysical Research: Oceans, 126, e2020JC016 977, https://doi.org/10.1029/2020JC016977, 2021.

Dupont, F., Dumont, D., Lemieux, J.-F., Dumas-Lefebvre, E., and Caya, A.: A Probabilistic Seabed–Ice Keel Interaction Model, The Cryosphere, 16, 1963–1977, https://doi.org/10.5194/tc-16-1963-2022, 2022.

Flato, G. M. and Hibler, W. D.: Ridging and Strength in Modeling the Thickness Distribution of Arctic Sea Ice, Journal of Geophysical Research: Oceans, 100, 18 611–18 626, https://doi.org/10.1029/95JC02091, 1995.

Haas, C., Pfaffling, A., Hendricks, S., Rabenstein, L., Etienne, J.-L., and Rigor, I.: Reduced Ice Thickness in Arctic Transpolar Drift Favors Rapid Ice Retreat, Geophysical Research Letters, 35, https://doi.org/10.1029/2008GL034457, 2008.

Haas, C., Lobach, J., Hendricks, S., Rabenstein, L., and Pfaffling, A.: Helicopter-Borne Measurements of Sea Ice Thickness, Using a Small and Lightweight, Digital EM System, Journal of Applied Geophysics, 67, 234–241, https://doi.org/10.1016/j.jappgeo.2008.05.005, 2009.

Hetenyi, M.: Beams on Elastic Foundation: Theory with Applications in the Fields of Civil and Mechanical Engineering, University of Michigan Press, 1946.

Hibler, W. D.: A Dynamic Thermodynamic Sea Ice Model, Journal of Physical Oceanography, 9, 815–846, https://doi.org/10.1175/1520-0485(1979)009<0815:adtsim>2.0.co;2, 1979.

Hibler, W. D.: Modeling a Variable Thickness Sea Ice Cover, Monthly Weather Review, 1980.

Hopkins, M. A.: On the Ridging of Intact Lead Ice, Journal of Geophysical Research: Oceans, 99, 16 351–16 360, https://doi.org/10.1029/94jc00996, 1994.

https://doi.org/10.5194/egusphere-2025-6421
Preprint. Discussion started: 27 January 2026

Hopkins, M. A.: The Effects of Individual Ridging Events on the Ice Thickness Distribution in the Arctic Ice Pack, Cold Regions Science and Technology, 24, 75–82, https://doi.org/10.1016/0165-232X(95)00006-W, 1996.

Hopkins, M. A.: Four Stages of Pressure Ridging, Journal of Geophysical Research: Oceans, 103, 21 883–21 891, https://doi.org/10.1029/98jc01257, 1998.

Hunke, E., Allard, R., Bailey, D. A., Blain, P., Craig, A., Dupont, F., DuVivier, A., Grumbine, R., Hebert, D., Holland, M., Jeffery, N., Lemieux, J.-F., Osinski, R., Rasmussen, T., Ribergaard, M., Roach, L., Roberts, A., Steketee, A., Turner, M., and Winton, M.: CICE-consortium/Icepack: Icepack 1.5.0, Zenodo, https://doi.org/10.5281/zenodo.14188409, 2024.

Hunke, E. C., Lipscomb, W. H., Turner, A. K., Jeffrey, N., and Elliott, S.: Cice: The Los Alamos Sea Ice Model Documentation and Software User's Manual Version 4.1 La-Cc-06-012, T-3 Fluid Dynamics Group, Los Alamos National Laboratory, 675, 500, https://doi.org/10.2172/1329842, 2010.

Hutter, N., Bouchat, A., Dupont, F., Dukhovskoy, D., Koldunov, N., Lee, Y. J., Lemieux, J.-F., Lique, C., Losch, M., Maslowski, W., Myers, P. G., Ólason, E., Rampal, P., Rasmussen, T., Talandier, C., Tremblay, B., and Wang, Q.: Sea Ice Rheology Experiment (SIREx): 2. Evaluating Linear Kinematic Features in High-Resolution Sea Ice Simulations, Journal of Geophysical Research: Oceans, 127, https://doi.org/10.1029/2021jc017666, 2022.

Johnson, M., Proshutinsky, A., Aksenov, Y., Nguyen, A. T., Lindsay, R., Haas, C., Zhang, J., Diansky, N., Kwok, R., Maslowski, W., Häkkinen, S., Ashik, I., and de Cuevas, B.: Evaluation of Arctic Sea Ice Thickness Simulated by Arctic Ocean Model Intercomparison Project Models, Journal of Geophysical Research: Oceans, 117, https://doi.org/10.1029/2011JC007257, 2012.

Krumpen, T., von Albedyll, L., Bünger, H. J., Castellani, G., Hartmann, J., Helm, V., Hendricks, S., Hutter, N., Landy, J. C., Lisovski, S., Lüpkes, C., Rohde, J., Suhrhoff, M., and Haas, C.: Smoother Sea Ice with Fewer Pressure Ridges in a More Dynamic Arctic, Nature Climate Change, 15, 66–72, https://doi.org/10.1038/s41558-024-02199-5, 2025.

Kulyakhtin and Høyland, K.: Distribution of Ice Block Sizes in Sails of Pressure Ice Ridges, in: The 22nd IAHR International Symposium on Ice, Proceedings of the 22nd IAHR International Symposium on Ice, pp. pages 235–240, 2014.

Lipscomb, W. H., Hunke, E. C., Maslowski, W., and Jakacki, J.: Ridging, Strength, and Stability in High-resolution Sea Ice Models, Journal of Geophysical Research: Oceans (1978–2012), 112, https://doi.org/10.1029/2005jc003355, 2007.

Liu, C., Kulkarni, K., Suominen, M., Kujala, P., and Musharraf, M.: On the Data-Driven Investigation of Factors Affecting the Need for Icebreaker Assistance in Ice-Covered Waters, Cold Regions Science and Technology, 221, 104 173, https://doi.org/10.1016/j.coldregions.2024.104173, 2024.

Mahoney, A., Eicken, H., and Shapiro, L.: How Fast Is Landfast Sea Ice? A Study of the Attachment and Detachment of Nearshore Ice at Barrow, Alaska, Cold Regions Science and Technology, 47, 233–255, https://doi.org/10.1016/j.coldregions.2006.09.005, 2007.

Mårtensson, S., Meier, H. E. M., Pemberton, P., and Haapala, J.: Ridged Sea Ice Characteristics in the Arctic from a Coupled Multicategory Sea Ice Model, Journal of Geophysical Research: Oceans, 117, https://doi.org/10.1029/2010JC006936, 2012.

Martin, T., Tsamados, M., Schroeder, D., and Feltham, D. L.: The Impact of Variable Sea Ice Roughness on Changes in Arctic Ocean Surface Stress: A Model Study, Journal of Geophysical Research: Oceans, 121, 1931–1952, https://doi.org/10.1002/2015JC011186, 2016.

Maus, S.: Bounds on the Initial Macroporosity of Sea Ice Pressure Ridges, Annals of Glaciology, 66, e10, https://doi.org/10.1017/aog.2025.4, 2025.

Maykut, G. A. and Untersteiner, N.: Some Results from a Time-Dependent Thermodynamic Model of Sea Ice, Journal of Geophysical Research (1896-1977), 76, 1550–1575, https://doi.org/10.1029/JC076i006p01550, 1971.

https://doi.org/10.5194/egusphere-2025-6421
Preprint. Discussion started: 27 January 2026

Melling, H. and Riedel, D. A.: Development of Seasonal Pack Ice in the Beaufort Sea during the Winter of 1991–1992: A View from Below, Journal of Geophysical Research: Oceans, 101, 11 975–11 991, https://doi.org/10.1029/96jc00284, 1996.

Metzger, A. T., Mahoney, A. R., and Roberts, A. F.: The Average Shape of Sea Ice Ridge Keels, Geophysical Research Letters, 48, e2021GL095 100, https://doi.org/10.1029/2021GL095100, 2021.

Muchow, M. and Polojärvi, A.: Three-Dimensional Discrete Element Simulations on Pressure Ridge Formation, The Cryosphere, 18, 4765–4774, https://doi.org/10.5194/tc-18-4765-2024, 2024.

Ólason, E., Boutin, G., Korosov, A., Rampal, P., Williams, T., Kimmritz, M., Dansereau, V., and Samaké, A.: A New Brittle Rheology and Numerical Framework for Large-Scale Sea-Ice Models, Journal of Advances in Modeling Earth Systems, 14, https://doi.org/10.1029/2021ms002685, 2022.

Petty, A. A., Tsamados, M. C., Kurtz, N. T., Farrell, S. L., Newman, T., Harbeck, J. P., Feltham, D. L., and Richter-Menge, J. A.: Characterizing Arctic Sea Ice Topography Using High-Resolution IceBridge Data, The Cryosphere, 10, 1161–1179, https://doi.org/10.5194/tc-10-1161-2016, 2016.

Roberts, A. F., Hunke, E. C., Kamal, S. M., Lipscomb, W. H., Horvat, C., and Maslowski, W.: A Variational Method for Sea Ice Ridging in Earth System Models, Journal of Advances in Modeling Earth Systems, 11, 771–805, https://doi.org/10.1029/2018ms001395, 2019.

Salganik, E., Høyland, K. V., and Maus, S.: Consolidation of Fresh Ice Ridges for Different Scales, Cold Regions Science and Technology, 171, 102 959, https://doi.org/10.1016/j.coldregions.2019.102959, 2020.

Sanderson, T. J. O.: Ice Mechanics and Risks to Offshore Structures, 1988.

Strub-Klein, L. and Sudom, D.: A Comprehensive Analysis of the Morphology of First-Year Sea Ice Ridges, Cold Regions Science and Technology, 82, 94–109, https://doi.org/10.1016/j.coldregions.2012.05.014, 2012.

Thorndike, A. S., Rothrock, D. A., Maykut, G. A., and Colony, R.: The Thickness Distribution of Sea Ice, Journal of Geophysical Research, 80, 4501–4513, https://doi.org/10.1029/jc080i033p04501, 1975.

Timco, G. W. and Burden, R. P.: An Analysis of the Shapes of Sea Ice Ridges, Cold Regions Science and Technology, 25, 65–77, https://doi.org/10.1016/S0165-232X(96)00017-1, 1997.

Todd, J.: Joeatodd/HiDEM: HiDEM v2.1.0, Zenodo, https://doi.org/10.5281/zenodo.1402603, 2018.

Tsamados, M., Feltham, D. L., Schroeder, D., Flocco, D., Farrell, S. L., Kurtz, N., Laxon, S. W., and Bacon, S.: Impact of Variable Atmospheric and Oceanic Form Drag on Simulations of Arctic Sea Ice, Journal of Physical Oceanography, https://doi.org/10.1175/JPO-D-13-0215.1, 2014.

Tuhkuri, J. and Lensu, M.: Laboratory Tests on Ridging and Rafting of Ice Sheets, Journal of Geophysical Research: Oceans (1978–2012), 107, 8–1–8–14, https://doi.org/10.1029/2001jc000848, 2002.

Uusinoka, M., Haapala, J., Åström, J., Lensu, M., and Polojärvi, A.: Scale invariance in kilometer-scale sea ice deformation, The Cryosphere, 19, 6493–6506, https://doi.org/10.5194/tc-19-6493-2025, 2025a.

Uusinoka, M., Savard, A., Åström, J., Haapala, J., and Polojärvi, A.: Threshold Domain Sizes for Multifractality in Sea Ice Deformation, Geophysical Research Letters, 52, e2025GL116 833, https://doi.org/10.1029/2025GL116833, 2025b.

Valdez Banda, O. A., Goerlandt, F., Montewka, J., and Kujala, P.: A Risk Analysis of Winter Navigation in Finnish Sea Areas, Accident Analysis & Prevention, 79, 100–116, https://doi.org/10.1016/j.aap.2015.03.024, 2015.

von Albedyll, L., Haas, C., and Dierking, W.: Linking Sea Ice Deformation to Ice Thickness Redistribution Using High-Resolution Satellite and Airborne Observations, The Cryosphere, 15, 2167–2186, https://doi.org/10.5194/tc-15-2167-2021, 2021.

https://doi.org/10.5194/egusphere-2025-6421
Preprint. Discussion started: 27 January 2026

von Albedyll, L., Hendricks, S., Grodofzig, R., Krumpen, T., Arndt, S., Belter, H. J., Birnbaum, G., Cheng, B., Hoppmann, M., Hutchings, J., Itkin, P., Lei, R., Nicolaus, M., Ricker, R., Rohde, J., Suhrhoff, M., Timofeeva, A., Watkins, D., Webster, M., and Haas, C.: Thermodynamic and Dynamic Contributions to Seasonal Arctic Sea Ice Thickness Distributions from Airborne Observations, Elementa: Science of the Anthropocene, 10, https://doi.org/10.1525/elementa.2021.00074, 2022.

Williams, T., Korosov, A., Rampal, P., and Ólason, E.: Presentation and Evaluation of the Arctic Sea Ice Forecasting System neXtSIM-F, The Cryosphere, 15, 3207–3227, https://doi.org/10.5194/tc-15-3207-2021, 2021.

Yu, Y., Maykut, G. A., and Rothrock, D. A.: Changes in the Thickness Distribution of Arctic Sea Ice between 1958–1970 and 1993–1997, Journal of Geophysical Research: Oceans, 109, https://doi.org/10.1029/2003JC001982, 2004.